Low-Cost High-Performance Generator for Testing Current Transformers Based on Frequency-Domain Feedback

Marco Faifer
DEIB
Politecnico di Milano
Milano, Italy
marco.faifer@polimi.it

Christian Laurano
DEIB
Politecnico di Milano
Milano, Italy
christian.laurano@polimi.it

Roberto Ottoboni
DEIB
Politecnico di Milano
Milano, Italy
roberto.ottoboni@polimi.it

Sergio Toscani
DEIB
Politecnico di Milano
Milano, Italy
sergio.toscani@polimi.it

***Abstract*—Characterizing the harmonic measurement performance of current transformers (CTs) requires a proper generator for applying realistic periodic current waveforms, mimicking those found in distribution grids. This paper proposes an approach for implementing a high-performance current generator, based on the usual, low-cost architecture consisting of a power amplifier, a transformer to boost its capability and a reference CT. Frequency-domain error feedback is adopted, with feedback gain set according to a preliminary frequency response measurement. This enables heavily mitigating the nonlinearity introduced by the current boost transformer, which no longer must be heavily overdesigned to reach high accuracy.**

***Index Terms*—Calibration, current measurement, current transformer (CT), harmonic distortion, power quality, power system harmonics**

I. Introduction

It is known for a long time that waveform distortion is among the most severe power quality phenomena in distribution grids (DGs). Harmonics increase power loss, accelerate aging, may energize resonances and cause inadvertent trip of protections [1]. Their magnitudes have significantly raised in the last years, because of the widespread diffusion of nonlinear devices, in particular those based on power electronics; the growth in the penetration of such devices is expected to continue in the next future [2], as a result of decarbonization.

Monitoring harmonics in DGs has paramount importance in this scenario: it would enable tracking their propagation [3], reconstructing the harmonic state of the grid [4] and attributing responsibilities for waveform distortion [5]. The trustworthiness of the results is directly connected to the quality of the incoming data, strongly dependent on the metrological characteristics of the adopted instrument transformers (ITs).

From a normative point of view, the role of ITs in harmonic measurements is recognized by the technical report [6]. Moreover, the recently revised standard [7] defines five optional accuracy class extensions, establishing performance requirements in the measurement of nonfundamental components. However, there is no reference procedure for accuracy assessment.

If ITs were exactly linear time invariant, accuracy would be fully defined by harmonic ratio and phase errors, independent from the spectral content of the primary waveform. This is not true in the presence of nonlinearity; alternative approaches have been proposed in [8] for voltage transformers (VTs) and in [9] for current transformers (CTs). Nonlinearity also makes that a concise accuracy indicator is unavoidably affected by the spectral content of the considered waveforms. For this reason, tests should be carried out with waveforms similar to those found during regular operation [10], [11]. Hence, it has key importance to have available a proper generator for applying periodic, distorted waveforms to the primary side of the IT under test. Such generator also enables identifying the parameters of processing methods for improving the harmonic measurement accuracy of ITs [12], [13].

Considering the characterization of inductive CTs, [14] proposes a method that avoids employing a high current source. It is an indirect approach, based on secondary-side injection that relies on the equivalent circuit of the transformer. In the other cases, a proper current generator is needed and two architectures can be adopted. The first uses a transconductance amplifier [15], [16]; while it enables to accurately control the applied current, it is rather expensive. In the second, lower-cost solution, the transconductance amplifier is replaced by a power amplifier (PA) feeding a transformer for increasing its output current [17], [18]. The drawback is that the generated current is far from being a scaled replica of the PA input. A possible solution is measuring the frequency response function (FRF) of the generation system, while using it to pre-distort the PA input waveform [17], [19]. Achieved performance heavily depends on the nonlinearities due to transformer core magnetization; hence, high accuracy demands for an overdesigned current boost transformer, operating at very low flux density and/or adopting a special core material, thus increasing cost.

Generation accuracy can be enhanced through feedback: a

This work was funded by European Union – Next Generation EU through the Italian Ministerial grant PRIN 2022 "Next-generation distributed synchronized measurement systems for smart grids with self-diagnostics capabilities and self-improvement of information quality," n. 2022RYZJT9, CUP D53D23001470006.

closed-loop (CL) controller may adjust the PA input according to the instantaneous deviation between measured and desired current. However, the design of such controller is extremely critical: both accuracy and stability heavily depend on it and its interaction with the generation system, including the load at the secondary side of the current boost transformer.

The present paper proposes improving accuracy through frequency-domain feedback: the harmonic phasors defining the PA input are iteratively adjusted according to the measured generation error at each component. It is demonstrated that stability and performance are guaranteed if feedback gain reflects the FRF of the generator, which has to be measured also for OL operation. Experimental results show the remarkable accuracy improvement, which is a step towards the implementation of a calibrator for distorted current waveforms.

II. Conventional Open-Loop Current Generator

The target of the current generator is feeding the primary side of the CT under test with realistic waveforms, resembling those found in DGs. Such waveforms can be considered periodic with fundamental frequency f_0, thus they can be written in terms of Fourier series. Therefore, assuming that the spectral content is bounded to the Hth order harmonic, the expression of the generic current to be generated results

$$i_{\text{ref}}(t) = \sqrt{2}\sum_{h=1}^{H} \Re\left\{\bar{I}_{\text{ref}}(h)\cdot e^{j2\pi h f_0 t}\right\} \tag{1}$$

where $\bar{\cdot}$ denotes complex-valued quantities, while $\bar{I}_{\text{ref}}(h)$ is the phasor of the hth order harmonic current. $i_{\text{ref}}(t)$ is thus defined by the column vector of the harmonic phasors, namely

$$\bar{\mathbf{i}}_{\text{ref}} = \begin{bmatrix}\bar{I}_{\text{ref}}(1) & \cdots & \bar{I}_{\text{ref}}(H)\end{bmatrix}^{\intercal} \tag{2}$$

condensing its one-sided spectrum. The current generator architecture adopted in [17] is considered, consisting of a PA whose output supplies a transformer that enables increasing its current capability. In turn, the secondary side of the transformer feeds the CT under test, while the generated current $i(t)$ is monitored through a reference transducer. The PA should be driven so that $i(t)$ is as close as possible to $i_{\text{ref}}(t)$.

The relationship between the PA input voltage $v(t)$ and $i(t)$ can be considered as nonlinear time invariant, where nonlinearity is mostly introduced by transformer core magnetization. Excluding chaotic phenomena (such as bifurcations and limit cycles) the steady-state response to a periodic input $v(t)$ with fundamental frequency f_0 is a periodic current $i(t)$ having the same fundamental frequency. The relationship between the harmonic phasors of the steady-state generated current (namely the elements of $\bar{\mathbf{i}}$, defined in the same fashion as $\bar{\mathbf{i}}_{\text{ref}}$ in (2)) and those of the input voltage (namely the components of $\bar{\mathbf{v}}$) can be written in the form

$$\bar{\mathbf{i}} = \bar{\mathbf{g}}(\bar{\mathbf{v}}) \tag{3}$$

where $\bar{\mathbf{g}}(\cdot)$ is a complex-valued vector function of a complex-valued vector argument. Ideally, if one exactly knows the behavior of the voltage generator, it would be possible to obtain the desired current by feeding the PA with a periodic input voltage whose harmonic phasors are the entries of $\bar{\mathbf{v}}_{\text{ref}} = \bar{\mathbf{g}}^{-1}(\bar{\mathbf{i}}_{\text{ref}})$. Having assumed that the PA operates within its rated capability and that the core flux density of the current boost transformer is well below saturation, nonlinearity is rather weak. The behavior can thus be approximated as linear time invariant, and the generic hth order harmonic phasor of the PA input is chosen as

$$\bar{V}(h) = \bar{Z}(h)\cdot\bar{I}_{\text{ref}}(h). \tag{4}$$

$\bar{Z}(h)$ represents an estimate of the FRF between generated current and input voltage, evaluated at frequency hf_0. In this case, the vector of the generated harmonic phasors is

$$\bar{\mathbf{i}} = \bar{\mathbf{g}}\left(\text{diag}(\bar{\mathbf{z}})\cdot\bar{\mathbf{i}}_{\text{ref}}\right) = \bar{\mathbf{i}}_{\text{ref}} + \Delta\bar{\mathbf{i}} \tag{5}$$

with $\Delta\bar{\mathbf{i}}$ being the vector of the deviations between generated and desired current phasors, namely the harmonic current errors that quantify achieved accuracy. Moreover $\bar{\mathbf{z}} = \begin{bmatrix}\bar{Z}(1) & \cdots & \bar{Z}(H)\end{bmatrix}^{\intercal}$ while $\text{diag}(\bar{\mathbf{z}})$ is a diagonal matrix whose main diagonal corresponds to $\bar{\mathbf{z}}$.

$\Delta\bar{\mathbf{i}}$ is nonzero since $\bar{\mathbf{z}}$ is an estimate, unavoidably subject to both measurement and definitional uncertainty, the latter due to the fact that we are representing the behavior of a nonlinear system with a linear model. Different approaches can be used to obtain $\bar{\mathbf{z}}$, each leading to a slightly different result; for example, it can be computed as the maximum likelihood estimate of the small-signal FRF of the generation system evaluated in the set of harmonic frequencies [20], or as the best linear approximation [21], [20] of the relationship between PA input and generated current phasors, for a predetermined class of periodic current waveforms [17].

III. Proposed Frequency-Domain Feedback Current Generator

As highlighted in the introduction, the performance achievable with the previously described current generator architecture is bounded by how well a FRF may represent the relationship between input voltage and generated current phasors. Therefore, tightening accuracy requires changing the hardware, namely adopting a current boost transformer having a more linear behavior, thus bulkier and more expensive.

The target of the present paper is removing the uncertainty contribution induced by the underlying linear representation of the generator. Ideally, performance shall be solely bounded by the output current measurement accuracy. In order to approach this goal, frequency-domain feedback is adopted. The harmonic phasors defining the PA input are iteratively updated according to the previous deviations between generated and desired current phasors, measured under steady-state conditions. In terms of equations, indicating with r the iteration index

$$\bar{\mathbf{v}}^{[r]} = \bar{\mathbf{v}}^{[r-1]} - \bar{\mathbf{K}}\cdot\Delta\bar{\mathbf{i}}^{[r-1]} \tag{6}$$

where $\Delta\bar{\mathbf{i}}^{[r-1]} = \bar{\mathbf{i}}^{[r-1]} - \bar{\mathbf{i}}_{\text{ref}}$, while $\bar{\mathbf{K}}$ is the feedback gain matrix. The CL behavior can be analyzed using the discrete-time systems theory. For the purpose it is worth introducing

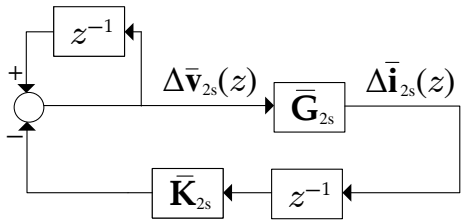

Fig. 1. Block diagram of the proposed closed-loop current generator.

$\Delta\bar{\mathbf{v}}^{[r]} = \bar{\mathbf{v}}^{[r]} - \bar{\mathbf{v}}_{\text{ref}}$, namely the vector of the deviations between the harmonic phasors defining the PA input at the rth iteration and those that would have resulted in $\Delta\bar{\mathbf{i}} = \mathbf{0}$. $\Delta\bar{\mathbf{v}}^{[r]}$ is hopefully small, hence (3) can be linearized around $\bar{\mathbf{v}}_{\text{ref}}$. In general $\mathbf{g}(\cdot)$ is non-holomorphic [22]: from the theory of nonlinear time invariant systems, an output phasor depends on all the input phasors as well as their complex conjugates [23]. Therefore, we have

$$\bar{\mathbf{i}}^{[r]} \approx \bar{\mathbf{i}}_{\text{ref}} + \bar{\mathbf{G}}_{+} \cdot \Delta\bar{\mathbf{v}}^{[r]} + \bar{\mathbf{G}}_{-} \cdot \Delta\underline{\mathbf{v}}^{[r]} \tag{7}$$

where

$$\bar{\mathbf{G}}_{+} = \left.\frac{\partial\bar{\mathbf{g}}}{\partial\bar{\mathbf{v}}}\right|_{\bar{\mathbf{v}}=\bar{\mathbf{v}}_{\text{ref}}} \qquad \bar{\mathbf{G}}_{-} = \left.\frac{\partial\bar{\mathbf{g}}}{\partial\underline{\mathbf{v}}}\right|_{\bar{\mathbf{v}}=\bar{\mathbf{v}}_{\text{ref}}}. \tag{8}$$

For the sake of convenience, it is worth introducing

$$\bar{\mathbf{v}}_{2s}^{[r]} = \begin{bmatrix}\bar{\mathbf{v}}^{[r]} \\ \underline{\mathbf{v}}^{[r]}\end{bmatrix} \qquad \bar{\mathbf{i}}_{2s}^{[r]} = \begin{bmatrix}\bar{\mathbf{i}}^{[r]} \\ \underline{\mathbf{i}}^{[r]}\end{bmatrix} \tag{9}$$

thus representing the two-sided spectral content of the PA input and generated current, respectively; $\Delta\bar{\mathbf{v}}_{2s}^{[r]}$ and $\Delta\bar{\mathbf{i}}_{2s}^{[r]}$ are defined analogously. Using the z-transform, it is possible to derive the block diagram of the CL generator in the neighborhood of the reference operating point. It is shown in Fig. 1, where

$$\bar{\mathbf{G}}_{2s} = \begin{bmatrix}\bar{\mathbf{G}}_{+} & \bar{\mathbf{G}}_{-} \\ \underline{\mathbf{G}}_{-} & \underline{\mathbf{G}}_{+}\end{bmatrix} \qquad \bar{\mathbf{K}}_{2s} = \begin{bmatrix}\bar{\mathbf{K}} & \underline{\mathbf{K}} \\ \bar{\mathbf{K}} & \underline{\mathbf{K}}\end{bmatrix}. \tag{10}$$

The behavior of the current generation error over the different iterations is ruled by the following linear, autonomous, discrete-time dynamical system

$$\Delta\bar{\mathbf{i}}_{2s}^{[r]} = \bar{\mathbf{A}} \cdot \Delta\bar{\mathbf{i}}_{2s}^{[r-1]} \tag{11}$$

$$\bar{\mathbf{A}} = \begin{bmatrix}\mathbf{1} - \bar{\mathbf{G}}_{+} \cdot \bar{\mathbf{K}} & -\bar{\mathbf{G}}_{-} \cdot \underline{\mathbf{K}} \\ -\underline{\mathbf{G}}_{-} \cdot \bar{\mathbf{K}} & \mathbf{1} - \underline{\mathbf{G}}_{+} \cdot \underline{\mathbf{K}}\end{bmatrix} \tag{12}$$

with $\mathbf{1}$ being the $H \times H$ identity matrix. Considering an initial generation error $\Delta\bar{\mathbf{i}}_{2s}^{[0]}$, the closed-form solution of (11) is

$$\Delta\bar{\mathbf{i}}_{2s}^{[r]} = \bar{\mathbf{A}}^{r} \cdot \Delta\bar{\mathbf{i}}_{2s}^{[0]}. \tag{13}$$

Hence, for a given harmonic order, the error at the rth iteration is a linear combination of rth powers of the eigenvalues of $\bar{\mathbf{A}}$. Necessary and sufficient condition for asymptotic stability is that all the magnitudes of such eigenvalues are below one. This implies that the harmonic current error fades to zero as $r \to \infty$; the smaller the magnitudes of the eigenvalues, the faster the decrease.

Performance depends on $\bar{\mathbf{A}}$ and thus, reminding (12), on the choice of the gain matrix $\bar{\mathbf{K}}$ with respect to the OL behavior of the current generator in the neighborhood of the operating point, assumed to be weakly nonlinear. Therefore, $\bar{\mathbf{G}}_{+}$ is almost diagonal: reminding (7), off-diagonal elements in the lth row are purely due to nonlinearity, since they model the variation of the current generation error at the lth order harmonic due to the variations of the PA input voltage phasors whose harmonic orders differ from l. Matrix $\bar{\mathbf{G}}_{-}$ is also purely connected to nonlinearity, taking into account the change of the current generation error at the different harmonics produced by the variations of the conjugates of the PA input voltage harmonic phasors; their entries are thus much smaller than those on the diagonal of $\bar{\mathbf{G}}_{+}$.

A particularly interesting choice is setting the gain matrix according to an estimate of the OL FRF between $v(t)$ and $i(t)$ on the harmonic grid (that adopted for conventional OL operation) hence $\bar{\mathbf{K}} = \text{diag}(\bar{\mathbf{z}})$. In this case, having initialized $\Delta\bar{\mathbf{i}}^{[0]} = -\bar{\mathbf{i}}_{\text{ref}}$, the first iteration reaches exactly the same operating point as the OL approach described in Section II. Moreover, by manipulating (12), it can be shown that $\bar{\mathbf{A}}$ corresponds to the relative deviation of the actual small-signal, frequency-domain behavior of the generation system with respect to the measured FRF. Therefore, if such FRF estimate provides a reasonably good approximation of the OL behavior, $\bar{\mathbf{G}}_{+}$ is close to be the inverse of $\text{diag}(\bar{\mathbf{z}})$.

Bounds for the magnitudes of the eigenvalues of $\bar{\mathbf{A}}$ can be obtained from the Gershgorin circle theorem [24]. Let us introduce $\bar{a}_{l,m}$ as the generic element of $\bar{\mathbf{A}}$ and R_l as the sum of the magnitudes of the non-diagonal entries in the lth row. All the eigenvalues of $\bar{\mathbf{A}}$ lie in at least a disc centered in $\bar{a}_{l,m}$ with radius R_l. Hence, if the measured FRF mimics the local OL behavior of the generator in the neighborhood of $\bar{\mathbf{i}}_{\text{ref}}$ within few percentage points, it also roughly corresponds to the order of magnitude of the eigenvalues of $\bar{\mathbf{A}}$. This guarantees CL stability, as well as a steep decrease of the current generation error within few iterations.

IV. Experimental Activity

A. Experimental Setup

The hardware architecture of the experimental setup implementing the improved current generator is shown in Fig. 2. It adopts a commercial, low-cost audio PA and a $5\,\text{A}/50\,\text{A}$ transformer to increase its maximum output current capability, with its secondary side feeding the CT under test. Generated current $i(t)$ is measured with a calibrated reference coaxial shunt, whose output voltage is scaled-up by an Analog Devices AD215BY insulation amplifier having a nominal gain of 100. Its frequency response has been measured and compensated, and the overall current measurement accuracy is better than $0.02\,\%$ in magnitude and $0.2\,\text{mrad}$ in terms of phase. The current waveform is acquired with rate $f_s = 200\,\text{kHz}$ by means of a National Instruments USB-6356 board, also providing the PA input voltage $v(t)$ thanks to the simultaneous sampling and generation capability. Acquisition, processing and generation are managed by a PC. It is worth highlighting that the proposed

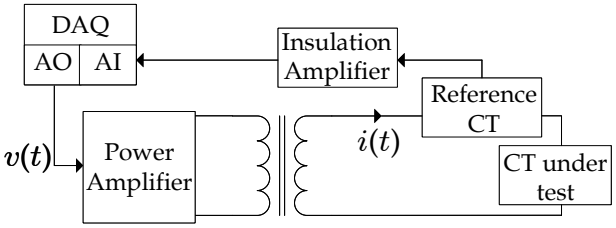

Fig. 2. Hardware architecture of the implemented current generator.

technique is based on successive offline updates of the PA input voltage. Hence, it does not lead to strict requirements in terms of computational power.

B. Class of reference current waveforms

In principle, the proposed current generator allows injecting any band-limited periodic current (so that it can be expressed in the form (1)) complying with the capabilities of the adopted equipment. Nevertheless, in this paper we investigate the achieved accuracy in generating waveforms similar to those found in DGs. In this respect, a class of periodic reference currents having $f_0 = 50\,\text{Hz}$ fundamental frequency (thus corresponding to 4000 samples per period) is introduced, defined in terms of probability density functions (pdfs) of harmonic amplitudes and phases. Fundamental magnitude is uniformly distributed between $5\,\%$ and $120\,\%$ of the rated current ($50\,\text{A}$), which is the measurement range for CTs [25]. Relative harmonic amplitudes (up to the 32nd order) are independent and uniformly distributed up to the limits reported in the standard [26] for devices with rated current greater than $16\,\text{A}$ not subject to conditional connection. Phases are independent with rectangular pdfs in $[-\pi, \pi)$.

C. Experimental Results

The first step is defining $\bar{\mathbf{z}}$, thus the feedback gain. For the purpose, a random-phase periodic multisine voltage has been applied to the input of the PA. It has $f_0 = 50\,\text{Hz}$ fundamental frequency and harmonics up to $H = 32$, all having the same magnitude so that the rms value of the resulting current is about $10\,\%$ of the rated value. $P = 100$ steady-state periods of the generated current have been measured, and the harmonic phasors have been extracted by computing the fast Fourier transform (FFT) on each period and averaging the P results. $\bar{\mathbf{z}}$ is then obtained as the maximum likelihood estimate of the generator FRF on the harmonic grid [20].

After that, a set of $S = 500$ reference current waveforms (each parametrized by a vector $\bar{\mathbf{i}}_{\text{ref}}^{[s]}$, $s \in \{1, \ldots, S\}$) has been built by sampling the pdfs defined in Section IV-B. For every sth reference current, $R = 5$ iterations have been considered. The generated current phasors corresponding to the rth iteration (with $r \in \{1, \ldots, R\}$), namely the entries of $\bar{\mathbf{i}}^{[r,s]}$, have been obtained by observing $P = 100$ steady-state periods, adopting the previously described procedure based on *per period* FFT computation and averaging. It is worth reminding that $r = 1$ corresponds to the usual OL operation.

Generation accuracy is quantified by evaluating $\Delta\bar{\mathbf{i}}^{[r,s]} = \bar{\mathbf{i}}^{[r,s]} - \bar{\mathbf{i}}_{\text{ref}}^{[s]}$, whose hth entry is $\Delta\bar{I}^{[r,s]}(h)$, namely the deviation between measured and desired harmonic phasor. If $\bar{I}^{[r,s]}(h)$ were measured with negligible uncertainty, this current deviation would correspond to the harmonic generation error. In order to obtain an overall performance indicator for a given harmonic order and iteration index, the following figure of merit is introduced

$$\xi^{[r]}(h) = \sqrt{\frac{\sum_{s=1}^{S} |\Delta\bar{I}^{[r,s]}(h)|^2}{\sum_{s=1}^{S} |\bar{I}_{\text{ref}}^{[s]}(h)|^2}} \tag{14}$$

which is the ratio between rms value of the hth order harmonic current deviation and the rms value of the hth order harmonic reference current, computed over the S signals. Values are reported in Fig. 3.

The figure highlights the remarkable performance enabled by the proposed approach, with ξ exhibiting a decreasing trend over the iterations. When considering $r = 1$, corresponding to OL operation, ξ is between $0.5\,\%$ up to above $4\,\%$, with the highest value corresponding to the 2nd order harmonic. The strongest reduction occurs with the first error feedback, thus moving to $r = 2$. In most cases, ξ stabilizes in the next two iterations, but for some harmonics (including the fundamental, the 3rd and few others) we notice a meaningful

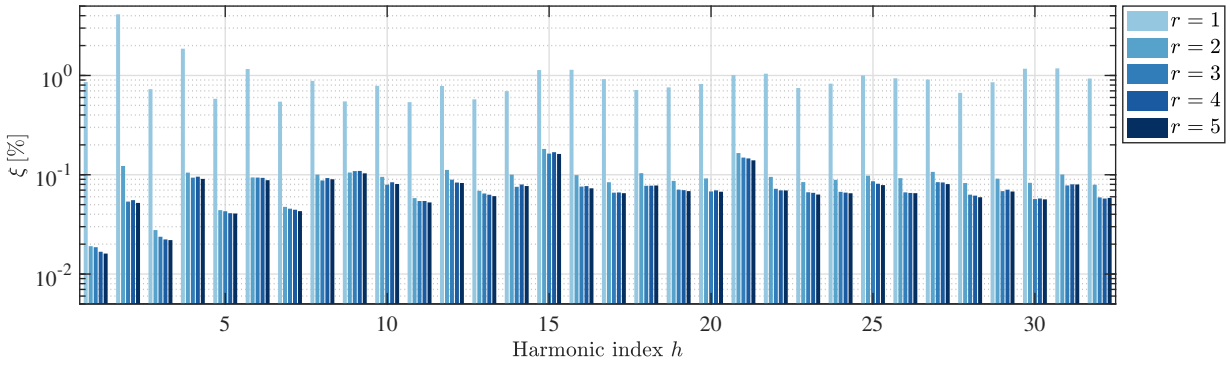

Fig. 3. Value of ξ for each harmonic order h and iteration step r.

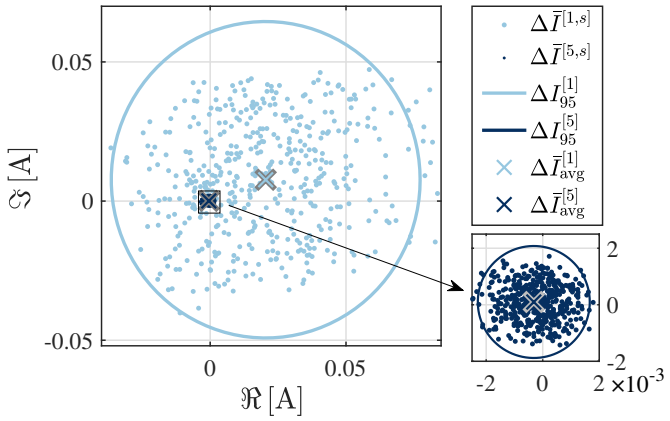

Fig. 4. Scatter plot of $\Delta\bar{I}^{[r,s]}(3)$, its average value and 95th percentile circumference for $r = 1$ and $r = 5$.

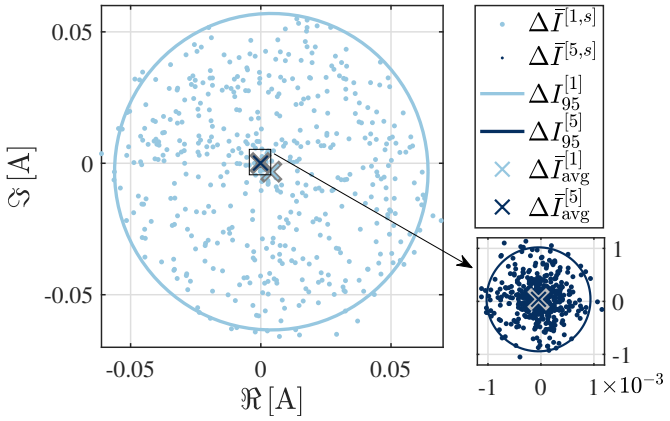

Fig. 5. Scatter plot of $\Delta\bar{I}^{[r,s]}(2)$, its average value and 95th percentile circumference for $r = 1$ and $r = 5$.

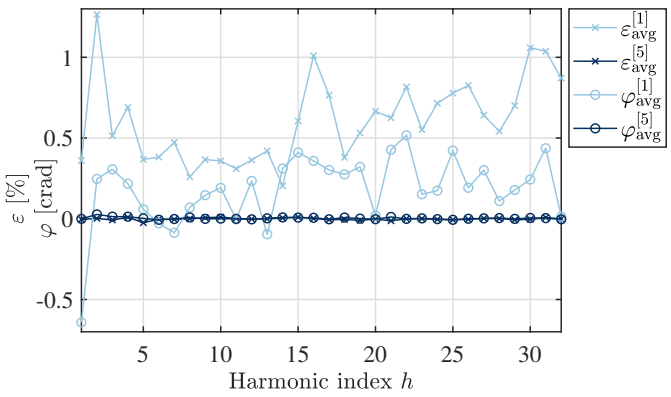

Fig. 6. Average values of magnitude and phase deviations for each harmonic order h, $r = 1$ and $r = 5$.

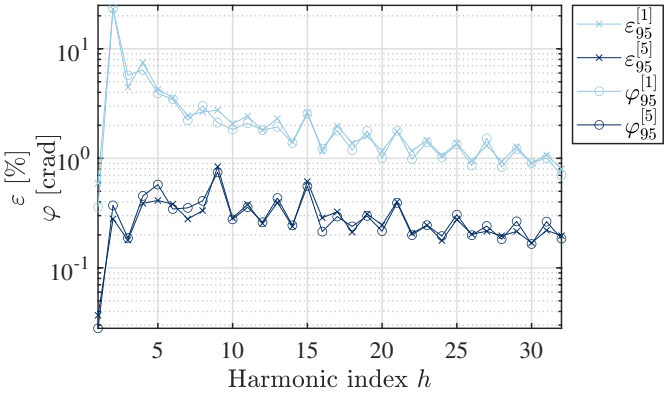

Fig. 7. 95th percentile bounds of magnitude and phase deviations for each harmonic order h, $r = 1$ and $r = 5$.

reduction even with $r = 5$. Anyway, CL operation enables decreasing ξ by at least an order of magnitude. For example, it reaches $0.05\,\%$ at the 2nd order harmonic, remaining below $0.1\,\%$ for all the components, except for the 15th and 21st order harmonics. For each iteration and harmonic index, the average value of the current deviation ($\Delta\bar{I}_{\text{avg}}^{[r]}(h)$) and the radius of the circumference centered on it including $95\,\%$ of the occurrences ($\Delta I_{95}^{[r]}(h)$) have been computed. Figure 4 reports the scatter plot of the $S = 500$ current deviations at the 3rd order harmonic, together with their average and 95th percentile circumference under OL operation ($r = 1$) and after the last iteration ($r = 5$). The accuracy improvement achieved thanks to frequency-domain feedback is evident. Considering $r = 1$, the average deviation is non-negligible (magnitude is about $2.2 \cdot 10^{-2}$ A) and the 95th percentile circumference has $5.7 \cdot 10^{-2}$ A radius. The cause is nonlinearity introduced by the boost transformer, in particular by the interaction with the large fundamental. Thanks to CL operation, the current deviation becomes zero-mean (magnitude is $3{\cdot}10^{-4}$ A) and circularly symmetric, with 95th percentile circumference having $2{\cdot}10^{-3}$ A radius, thus reduced by a factor 30. It is worth showing also the scatter plot of the current deviations at the 2nd order harmonic, characterized by the highest value of ξ under OL operation; results are depicted in Fig. 5. Considering OL operation, current deviation is slightly biased (average value has $5{\cdot}10^{-3}$ A magnitude) and the 95th percentile circumference has a radius of 0.06 A. Such behavior is mainly due to the intermodulation between the fundamental component and the dc current produced by the PA output offset. Frequency-domain feedback results in virtually unbiased current deviation (the magnitude of the average is $3.1 \cdot 10^{-5}$ A), whose 95th percentile circumference has $1 \cdot 10^{-3}$ A radius.

Accuracy is typically expressed in terms of magnitude and phase deviations (indicated with ε and φ, respectively) corresponding to magnitude and phase errors if the uncertainty contribution of the reference CT were negligible. For each harmonic order h and iteration step r, their average values ($\varepsilon_{\text{avg}}^{[r]}(h)$ and $\varphi_{\text{avg}}^{[r]}(h)$) and 95th percentile bounds centered on the average ($\varepsilon_{95}^{[r]}(h)$ and $\varphi_{95}^{[r]}(h)$) have been computed. Figure 6 reports the average deviations while Fig. 7 shows the 95th percentile bounds both under OL operation ($r = 1$) and after the last iteration ($r = 5$). Having expressed the magnitude deviation as percentage and the phase deviation in centiradians, they can be plot on the same scale. Consider-

ing OL operation, Fig. 6 shows significantly biased values, with the maximum average magnitude deviation exceeding $1.2\,\%$ at the 2nd order harmonic (induced by the PA output offset) and the highest average phase deviation of $-0.7\,\mathrm{crad}$ occurring at the fundamental. On the other hand, frequency-domain error feedback results in negligible bias for both magnitude and phase deviations. Figure 7 firstly shows how the 95th percentile bounds of magnitude and phase deviations are extremely similar (both for $r = 1$ and $r = 5$) as a result of the nearly circularly symmetric distribution of the current deviation around its average value. This figure also quantifies the large accuracy improvement enabled by CL operation; a logarithmic scale has been adopted to deal with the large reduction. As an example, considering $r = 1$, the highest 95th percentile values occur at the 2nd order harmonic, exceeding $20\,\%$ and $20\,\mathrm{crad}$ as a result of the PA output offset, while exhibiting a roughly decreasing trend with frequency; anyway, values are always above $0.8\,\%$ and $0.8\,\mathrm{crad}$. Thanks to feedback, all the harmonic current deviations have the same order of magnitude, going from less than $0.2\,\%$ and $0.2\,\mathrm{crad}$ to $0.4\,\%$ and $0.4\,\mathrm{crad}$, except for the 9th and 15th order harmonics. It is worth noting that magnitude and phase deviations are highly correlated with the harmonic magnitude: in particular, the largest deviations always correspond to the smallest harmonic magnitudes.

V. Conclusion

Characterizing CTs adopted for harmonic measurements requires a generator capable of injecting realistic, distorted current waveforms with high accuracy. In this paper the performance achieved with a conventional low-cost current generator architecture, made of a PA coupled with a current boost transformer, has been greatly improved through frequency-domain feedback. The deviation between desired and measured output current quickly fades if feedback gain is set according to an OL FRF estimate of the generation system. Thanks to the proposed approach, nonlinearities introduced by the current boost transformer are heavily mitigated. Therefore, it enables reaching high generation accuracy (bounded by that of the reference current transducer) without employing an overdesigned and more expensive current boost transformer.

References

[1] J. Arrillaga and N. R. Watson, *Power System Harmonics*. Hoboken, NJ, USA: John Wiley & Sons, Ltd, 2003.

[2] H. Sharma, M. Rylander, and D. Dorr, "Grid impacts due to increased penetration of newer harmonic sources," *IEEE Transactions on Industry Applications*, vol. 52, no. 1, pp. 99–104, 2016.

[3] P. S. Wright, A. E. Christensen, P. N. Davis, and T. Lippert, "Multiple-site amplitude and phase measurements of harmonics for analysis of harmonic propagation on Bornholm island," *IEEE Transactions on Instrumentation and Measurement*, vol. 66, no. 6, pp. 1176–1183, 2017.

[4] A. Meliopoulos, F. Zhang, and S. Zelingher, "Power system harmonic state estimation," *IEEE Transactions on Power Delivery*, vol. 9, no. 3, pp. 1701–1709, 1994.

[5] F. Safargholi, K. Malekian, and W. Schufft, "On the dominant harmonic source identification— part i: Review of methods," *IEEE Transactions on Power Delivery*, vol. 33, no. 3, pp. 1268–1277, 2018.

[6] *Instrument transformers - The use of instrument transformers for power quality measurement*, IEC Technical Report IEC TR61869-103, 2012.

[7] *Instrument transformers - Part 1: General requirements*, IEC Int. Std. IEC 61869-1:2023, 2023.

[8] M. Faifer, A. Ferrero, C. Laurano, R. Ottoboni, S. Toscani, and M. Zanoni, "An innovative approach to express uncertainty introduced by voltage transformers," *IEEE Transactions on Instrumentation and Measurement*, vol. 69, no. 9, pp. 6696–6703, 2020.

[9] M. Faifer, C. Laurano, R. Ottoboni, and S. Toscani, "A new method to represent the harmonic measurement accuracy of current transformers," *IEEE Transactions on Instrumentation and Measurement*, vol. 73, pp. 1–11, 2024.

[10] G. Crotti, D. Gallo, D. Giordano, C. Landi, M. Luiso, and M. Modarres, "Frequency response of MV voltage transformer under actual waveforms," *IEEE Transactions on Instrumentation and Measurement*, vol. 66, no. 6, pp. 1146–1154, 2017.

[11] M. Faifer, C. Laurano, R. Ottoboni, S. Toscani, and M. Zanoni, "Characterization of voltage instrument transformers under nonsinusoidal conditions based on the best linear approximation," *IEEE Transactions on Instrumentation and Measurement*, vol. 67, no. 10, pp. 2392–2400, 2018.

[12] G. D'Avanzo, M. Faifer, C. Landi, C. Laurano, P. S. Letizia, M. Luiso, R. Ottoboni, and S. Toscani, "Theory and experimental validation of two techniques for compensating VT nonlinearities," *IEEE Transactions on Instrumentation and Measurement*, vol. 71, pp. 1–12, 2022.

[13] M. Faifer, C. Laurano, R. Ottoboni, and S. Toscani, "Adaptive polynomial harmonic distortion compensation in current and voltage transformers through iteratively updated QR factorization," *IEEE Transactions on Instrumentation and Measurement*, vol. 72, pp. 1–10, 2023.

[14] M. Kaczmarek and E. Stano, "New approach to evaluate the transformation accuracy of inductive CTs for distorted current," *Energies*, vol. 16, no. 7, 2023.

[15] B. Djokić and H. Parks, "Calibration of electrical instruments under nonsinusoidal conditions at NRC Canada," *IEEE Transactions on Instrumentation and Measurement*, vol. 70, pp. 1–6, 2021.

[16] F. Costa, A. Mingotti, L. Peretto, and R. Tinarelli, "Combined effect of temperature and humidity on distorted currents measured by Rogowski coils," in *2022 20th International Conference on Harmonics & Quality of Power (ICHQP)*, 2022, pp. 1–6.

[17] L. Cristaldi, M. Faifer, C. Laurano, R. Ottoboni, S. Toscani, and M. Zanoni, "A low-cost generator for testing and calibrating current transformers," *IEEE Transactions on Instrumentation and Measurement*, vol. 68, no. 8, pp. 2792–2799, 2019.

[18] M. Kaczmarek and P. Kaczmarek, "Comparison of the wideband power sources used to supply step-up current transformers for generation of distorted currents," *Energies*, vol. 13, no. 7, 2020. [Online]. Available: https://www.mdpi.com/1996-1073/13/7/1849

[19] M. Faifer, C. Laurano, R. Ottoboni, and S. Toscani, "Development of a low-cost three-phase current generator for testing current transformers," in *2023 IEEE 13th International Workshop on Applied Measurements for Power Systems (AMPS)*, 2023, pp. 01–06.

[20] R. Pintelon and J. Schoukens, *System Identification: A Frequency Domain Approach*. Hoboken, NJ, USA: Wiley-IEEE Press, 2012.

[21] J. Schoukens, T. Dobrowiecki, and R. Pintelon, "Parametric and nonparametric identification of linear systems in the presence of nonlinear distortions-a frequency domain approach," *IEEE Transactions on Automatic Control*, vol. 43, no. 2, pp. 176–190, 1998.

[22] A. Hjørungnes, *Complex-Valued Matrix Derivatives: With Applications in Signal Processing and Communications*. Cambridge, UK: Cambridge University Press, 2011.

[23] L. O. Chua and C.-Y. Ng, "Frequency domain analysis of nonlinear systems: general theory," *IEE Journal on Electronic Circuits and Systems*, vol. 3, pp. 165–185(20), July 1979.

[24] G. H. Golub and C. F. Van Loan, *Matrix Computations*, ser. Johns Hopkins Studies in the Mathematical Sciences. Baltimore, MD, USA: Johns Hopkins University Press, 1996.

[25] *Instrument transformers - Part 2: Additional requirements for current transformers*, IEC Int. Std. IEC 61869-2-:2012, 2012.

[26] *Electromagnetic compatibility (EMC) – Part 3.4: Limits. Limitation of emission of harmonic currents in low-voltage power supply systems for equipment with rated current greater than 16 A*, IEC Int. Std. IEC 61000-3-4:1998, 1998.